Evaluation of the influence of density in the acoustic waves amplitudes

Leandro Di Bartolo, Cleberson Dors, Webe João Mansur, Cid da Silva Garcia Monteiro (COPPE/UFRJ)

Abstract

It is a fact that real geological media present variations in density so due to stratigraphic or structural geological formations as due to the pressure exerted by the upper layers. This fact directly affects the recorded amplitudes in seismograms. Taking into account that the amplitudes are directly related to several parameters such as the reflection coefficient, porosity, etc, the correct representation of them is fundamental for the correct evaluation of the seismic attributes. In this context, the present work aims to evaluate the differences in the synthetic seismic amplitudes by comparing the wave field with and without consideration of the density contrasts.

INTRODUCTION

Due to continuous and growing expansion of the oil exploration horizons, the complex geological medium become common in the industry. Additionally, nowadays, the objective with the application of the seismic method is not only the mapping of geometric structures as it was early, but also the monitoring and characterization of reservatories. In this sense, the seismic modelling can therefore be divided into kinematic and dynamic, related to travel times and amplitudes. In the first case, the interest is only the geometric mapping of the reflects and, in the second case, the interest is also in seismic attributes, where the amplitudes play a key role.

Because of the growing complexity of the oil target, the use of formulations based on the full wave equation acquires central importance, not only for modelling but also for seismic migration, as the case of Reverse Time Migration (RTM). It is clear that the full wave equation, without any approximation, is suitable for a realistic representation of the wave field. However, the density gradient is often neglected in acoustic modelling and RTM and this can affect the amplitude results.

This paper aims to study how the amplitudes are changed during the propagation of acoustic waves due to the presence of density contrasts. To this purpose, was evaluated the deviations in the propagated waves amplitudes without taking into account the density contrast, compared with propagation that takes into account these contrasts. For this intent, were used two distinct approaches. The first involves the analytical study of simplified geological settings, to understand qualitatively and quantitatively these deviations, both in wave propagation in depth and in surface of the model (synthetic seismogram). The second approach verifies these deviations using finite difference numerical schemes applied to a complex geological model.

The paper is divided as follows: in the first section, equations describing the acoustic wave propagation are discussed and, subsequently, the different numerical formulations used to solve such equations are presented. The following section undertakes the analytical study of media composed by plane-parallel layers. Finally, two examples are present: the first involves four models of plane-parallel layers, in which numerical modelling are compared with the respective analytical solutions; and another involving the complex model known in literature as Marmousi Model. In the last section, the conclusions are presented.

ACOUSTIC WAVE PROPAGATION

The acoustic wave equation for general heterogeneous media is given by

$$\rho\vec{\nabla}.\left(\frac{1}{\rho}\vec{\nabla}p\right)-\frac{1}{c^2}\frac{\partial^2 p}{\partial t^2}=-\rho f, \tag{1}$$

where p is the acoustic pressure, f is the seismic source and $c=\sqrt{\kappa/\rho}$ is the speed propagation of wave in the medium, being ρ the density and κ the adiabatic compression modulus. For regions where the density gradient is negligible, the Eq. (1) can be simplified to

$$\nabla^2 p-\frac{1}{c^2}\frac{\partial^2 p}{\partial t^2}=-\rho f. \tag{2}$$

A variant of Eq. (1) is the first order system given by

$$\begin{aligned}\frac{1}{\kappa}\frac{\partial p}{\partial t}+\vec{\nabla}.\vec{v} &= f_2\\ \rho\frac{\partial\vec{v}}{\partial t}+\vec{\nabla}p &= 0,\end{aligned} \tag{3}$$

where $\vec{v}$ is the velocity vector of particles of the medium.

NUMERICAL FORMULATIONS

All numerical formulations implemented are based on the Finite Difference Method (FDM) in two-dimensional media, using the fourth order in space and the second order in time. It is remarkable that the formulation based on Eq. (2) will be referred to as homogeneous formulation (ρ constant) and those based on Eq. (1) and (3) are called heterogeneous (ρ variable), the latter also referred to as staggered.

Homogeneous Formulation

The first scheme implemented is widely known and used in geophysics, being the Eq. (2) discretized using the

following central difference approximations

$$\left(\frac{d^2p}{dx^2}\right)_i^k = \frac{4}{3}\frac{p_{i+1}^k - 2p_i^k + p_{i-1}^k}{h^2} - \frac{1}{3}\frac{p_{i+2}^k - 2p_i^k + p_{i-2}^k}{(2h)^2} \quad (4)$$

$$\left(\frac{\partial^2p}{\partial t^2}\right)_i^k = \frac{p_i^{k-1} - 2p_i^k + p_i^{k+1}}{\Delta t^2}, \quad (5)$$

where the index i refers to the spatial coordinates and the index k, to the time coordinate; h is the grid spacing and Δt, the time interval. Then, the scheme is obtained, replacing the Eq. (4) and (5) in Eq. (2) and expliciting p at time $k+1$ depending on the pressure field in earlier times.

Heterogeneous formulation

To discretize the Eq. (1), we use the scheme developed by Cohen and Joly (1996) in which the time derivative is approximated by Eq. (5) and the spatial derivatives, by fourth-order expressions given by

$$\left[\kappa\frac{\partial}{h}\left(\frac{1}{\rho}\frac{\partial p}{\partial x}\right)\right]_i^k = \frac{4\kappa_i}{3h}\left[b_{i+\frac{1}{2}}^{\lambda_{i+\frac{1}{2}}}\left(\frac{p_{i+1}^k - p_i^k}{h}\right) - b_{i-\frac{1}{2}}^{\lambda_{i-\frac{1}{2}}}\left(\frac{p_i^k - p_{i-1}^k}{h}\right)\right] - \frac{\kappa_i}{3(2h)}\left[b_{i+1}\left(\frac{p_{i+2}^k - p_i^k}{2h}\right) - b_{i-1}\left(\frac{p_i^k - p_{i-2}^k}{2h}\right)\right], \quad (6)$$

where κ and $b = 1/\rho$ are the properties of heterogeneous media and must be calculated through

$$\kappa_i = \frac{1}{2h}\int_{x_{i-1}}^{x_{i+1}} \kappa(x)dx \qquad \text{e} \qquad b_{i+\frac{1}{2}} = \frac{1}{h}\int_{x_i}^{x_{i+1}} b(x)dx\,, \quad (7)$$

being the properties $b_{i+\frac{1}{2}}^{\lambda_{i+\frac{1}{2}}}$ calculated using the average and the optimal parameter λ suggested in the cited article.

Staggered heterogeneous formulation

To discretize the system given by Eq. (3), it is applied a simplification of the Virieux (1986) formulation for the case of acoustics. Then, we use the following approximations for the spatial and temporal derivatives applied to p or $\vec{v}$ components, in fourth order in space and second order in time:

$$\left(\frac{\partial h}{\partial t}\right)_i^k = \frac{h_i^{k+1/2} - h_i^{k-1/2}}{\Delta t}, \quad (8)$$

$$\left(\frac{\partial h}{\partial x}\right)_i^k = \frac{-h_{i+3/2}^k + 27h_{i+1/2}^k - 27h_{i-1/2}^k + h_{i-3/2}^k}{24h}. \quad (9)$$

PLANE PARALLEL LAYERS MEDIUM

By Snell's Law, the ray path in a complex medium only depends on velocity field of propagation in this medium. Therefore, it is clear that the density contrasts only influence the amplitudes, not changing the path of the wave. Knowing the values of transmission and reflection coefficients along the paths of the rays, which represent each wavefront, with or without considering the gradient of density, one can calculate the ratios between the amplitudes in these cases.

Then, consider a model with n plane-parallel horizontal layers, each with properties given by v_i and ρ_i with $i = 1,2,\ldots,n$. In this model, first is applied a plane wave which moves in the z direction downward (Fig. 1-a), that is, with the horizontal wavefront.

Defining the following ratios between adjacent properties

$$\alpha_i = \frac{\rho_i}{\rho_{i+1}} \quad \text{e} \quad \beta_i = \frac{v_i}{v_{i+1}}, \quad (10)$$

the coefficients R_i of reflection and T_i of transmission, for each interface i, can be written as

$$R_i = \frac{a^R}{a^I} = \frac{Z_{i+1} - Z_i}{Z_i + Z_{i+1}} = \frac{1 - \alpha_i\beta_i}{1 + \alpha_i\beta_i} \quad (11)$$

$$T_i = \frac{a^T}{a^I} = \frac{2Z_{i+1}}{Z_i + Z_{i+1}} = \frac{2}{1 + \alpha_i\beta_i}, \quad (12)$$

where $Z_i = \rho_i v_i$ is the acoustic impedance of the layer i, and a^I, a^R e a^T are the amplitudes of the reflected and transmitted incident (downward) waves, respectively. By Equation (11), we can calculate the accumulated transmission coefficient A_i, corresponding to the propagation between the layer 1 and layer i, as

$$A_i = 2\prod_{j=1}^{i-1}\frac{1}{1 + \alpha_j\beta_j}. \quad (13)$$

This A_i factor corresponds to the ratio between the amplitude that reaches to the layer i and original amplitude (in the layer 1). Likewise, can be obtained an equation that expresses the accumulated transmission coefficient accumulated by upward wave, of the layer n to the first layer. Multiplying then by the accumulated transmission coefficients of the downward wave (until the layer i), by the reflection coefficient on the interface i and by the accumulated transmission coefficients of the upward wave, the following coefficient can be obtained

$$B_i = 4\left(\frac{1 - \alpha_i\beta_i}{1 + \alpha_i\beta_i}\right)\prod_{j=1}^{i-1}\frac{\alpha_j\beta_j}{(1 + \alpha_j\beta_j)^2}. \quad (14)$$

The coefficient B_i gives the ratio of the original amplitude (source) by the value of the amplitude of the wave that returns to the first layer, after it has been reflected at layer i.

The accumulated amplitude deviation caused by disregarding the density variations, respectively, for the downward wave at the layer i and for the upward wave returned to surface, are the r_i^A and r_i^B coefficients given by

$$r_i^A = \frac{A_i^{\rho\ cte}}{A_i^{\rho\ var}} = \prod_{j=1}^{i-1}\frac{1 + \alpha_j\beta_j}{1 + \beta_j} \quad (15)$$

$$r_i^B = \frac{B_i^{\rho\ cte}}{B_i^{\rho\ var}} = \frac{(1 + \alpha_i\beta_i)}{(1 + \beta_i)}\frac{(1 - \beta_i)}{(1 - \alpha_i\beta_i)}\prod_{j=1}^{i-1}\frac{(1 + \alpha_j\beta_j)^2}{\alpha_j(1 + \beta_j)^2}, \quad (16)$$

where $(A_i^{\rho\ cte}, A_i^{\rho\ var})$ and $(B_i^{\rho\ cte}, B_i^{\rho\ var})$ are given by Eq. (13) and (14), respectively, considering the density constant or not. The term outside the productory, in Eq. (16), is the error $r_i^R = R_i^{\rho\ cte}/R_i^{\rho\ var}$ caused by reflection.

Now, consider the oblique incidence of a plane wave in the model of layers (Fig. 1-b). Considering an interface i, the

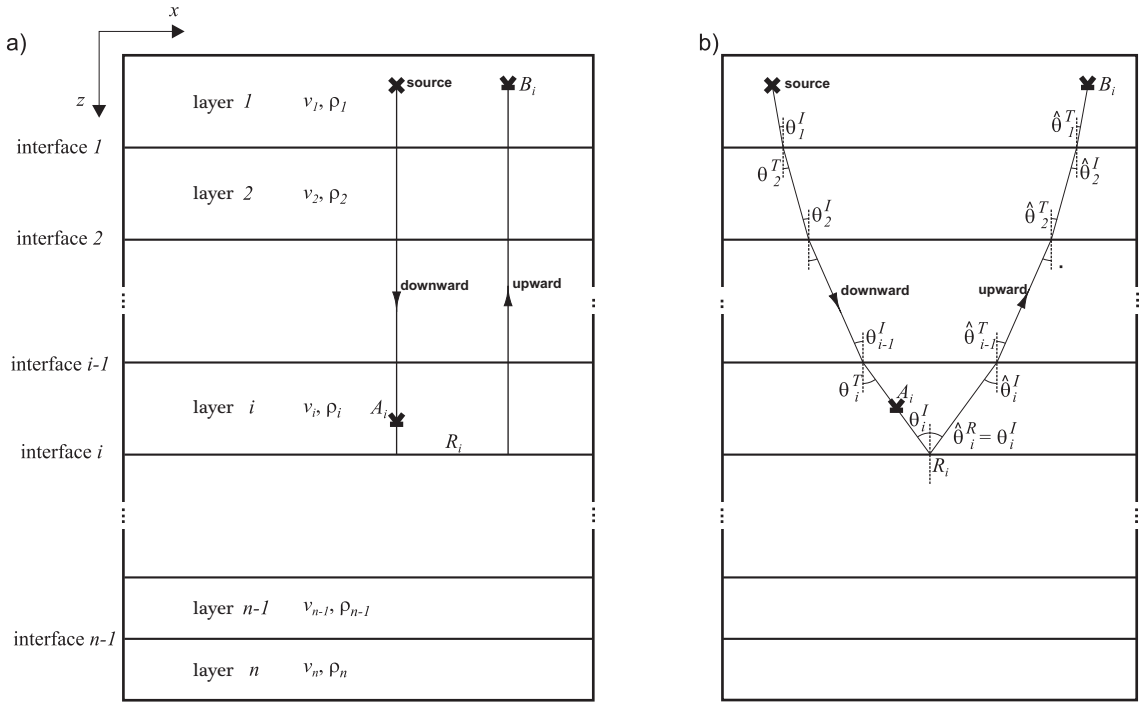

Figure 1: Plane-parallel layers model. In (a), it is showed a situation with perpendicular incidence and, in (b), with oblique incidence. Here, are showed the ray paths that descends and ascends and the A_i, B_i and R_i receptor positions, indicating where are measured the coefficients of the same name (see text). In addition, in (b) are showed the θ_i incidence and transmission angles (index I and T), for both downward (θ_i) and upward ($\hat{\theta}_i$) rays.

generalizations for the reflection ($\bar{R}_i$) and transmission ($\bar{T}_i$) coefficients are given by

$$\bar{R}_i = \frac{Z_{i+1}\cos\theta_i^I - Z_i\cos\theta_{i+1}^T}{Z_{i+1}\cos\theta_i^I + Z_i\cos\theta_{i+1}^T} = \frac{1-\alpha_i\beta_i\gamma_i}{1+\alpha_i\beta_i\gamma_i} \tag{17}$$

$$\bar{T}_i = \frac{2Z_{i+1}\cos\theta_i^I}{Z_{i+1}\cos\theta_i^I + Z_i\cos\theta_{i+1}^T} = \frac{2}{1+\alpha_i\beta_i\gamma_i}, \tag{18}$$

where $\gamma_i = \cos\theta_{i+1}^T/\cos\theta_i^I$, being θ_i^I and θ_{i+1}^T the angles of incidence and transmission. By the Snell's Law they are related by

$$\theta_{i+1}^T = \text{arcsen}\left(\text{sen}\,\theta_i^I/\beta_i\right). \tag{19}$$

It is important to note that in the case of plane-parallel layers $\theta_i^I = \theta_i^T$, $\hat{\theta}_i^I = \theta_i^T$ and $\hat{\theta}_i^T = \theta_i^I$ $\forall\, i$ (see Fig. 1-b). Additionally, it should be remembered that when the incidence angle θ_i^I is equal to or greater that the limit angle $\theta_i^{IL} = \text{arcsen}(\beta_i)$, there will be total reflection, not emerging transmitted wave in the layer $i+1$.

With that, from Equation (17) and (18), can be obtained the following generalization of Eq. (15) and (16):

$$\bar{r}_i^A = \frac{\bar{A}_i^{\rho\ cte}}{\bar{A}_i^{\rho\ var}} = \prod_{j=1}^{i-1}\frac{1+\alpha_j\beta_j\gamma_j}{1+\beta_j\gamma_j} \tag{20}$$

$$\bar{r}_i^B = \frac{\bar{B}_i^{\rho\ cte}}{\bar{B}_i^{\rho\ var}} = \frac{(1+\alpha_i\beta_i\gamma_i)(1-\beta_i\gamma_i)}{(1+\beta_i\gamma_i)(1-\alpha_i\beta_i\gamma_i)}\prod_{j=1}^{i-1}\frac{(1+\alpha_j\beta_j\gamma_j)^2}{\alpha_j(1+\beta_j\gamma_j)^2}, \tag{21}$$

Like the Eq. (15) and (16), the Eq. (20) and (21) are also valid for punctual sources applied to model layer plane-parallel, since the decaiment factor of the amplitude due to the spherical spreading of the wavefront is the same with or without considering the density contrast.

Analysis of the analytical expressions

Next, the analytical values of the $\bar{r}_i^A$ coefficients (in depth) and $\bar{r}^B$ coefficients (on the surface) have been evaluated, as explained above, for the four models of 15 layers (Tab. 1). The contrasts of density and velocity models

Table 1: Properties of the layers models (in SI units).

l	model 1		model 2		model 3		model 4	
	ρ	v	ρ	v	ρ	v	ρ	v
1	1000	1500	1000	1500	1750	1600	1750	1600
2	1800	1800	1800	1800	1800	1800	1800	1800
3	1850	2000	1900	2200	1850	2000	1900	2200
4	1900	2200	1850	2000	1900	2200	1850	2000
5	1950	2400	1950	2400	1950	2400	1950	2400
6	2000	2600	2050	2800	2000	2600	2050	2800
7	2050	2800	2000	2600	2050	2800	2000	2600
8	2100	3000	2100	3000	2100	3000	2100	3000
9	2150	3200	2200	3400	2150	3200	2200	3400
10	2200	3400	2150	3200	2200	3400	2150	3200
11	2250	3600	2250	3600	2250	3600	2250	3600
12	2300	3800	2350	4000	2300	3800	2350	4000
13	2350	4000	2300	3800	2350	4000	2300	3800
14	2400	4200	2400	4200	2400	4200	2400	4200
15	2450	4400	2450	4400	2450	4400	2450	4400

are typical of geophysical media, where models 1 and 2 are offshore models and models 3 and 4 are onshore models. In the models 2 and 4 there is change in position of adjacent layers.

The analytical $\bar{r}_i^A$ and $\bar{r}_i^B$ coefficients, respectively, in the depth and at surface in function of layer i and of the angle of incidence in the first interface are shown in Fig. 2

(offshore models) and 3 (onshore models). In both cases,

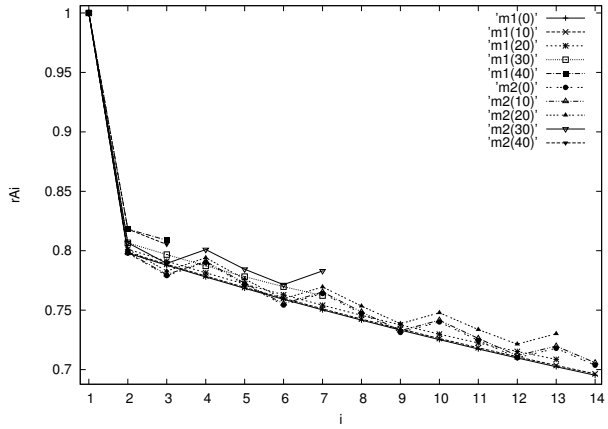

Figure 2: Coefficients $\bar{r}_i^A$ of models 1 and 2 (m1 and m2) per interface. Each curve shows the variation $\bar{r}_i^A$ along the i layers for different angles of incidence at the first interface, in degrees (m1(θ_1^I)).

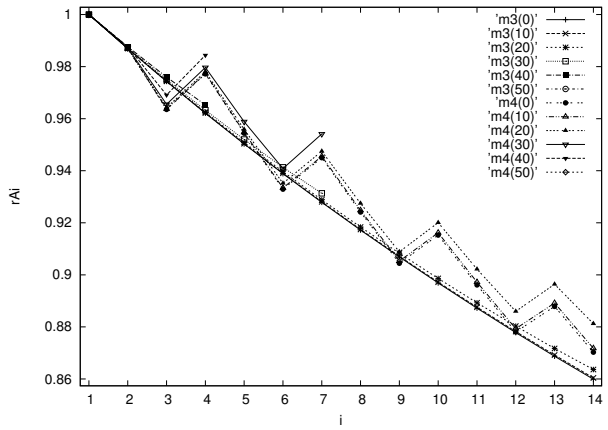

Figure 3: Coefficients $\bar{r}_i^A$ of models 3 e 4 (m3 and m4) per interface, following the Fig. 2.

the error increases as more density contrasts are crossed, so it increases with depth. Typically, for models 1 and 2 (offshore) the amplitude error is 20 % in the first interface, increasing linearly layer by layer. For the models 3 and 4 (onshore), it is remarkable that these differences become more significant for the deepest layers (around 15 %). It is emphasized that in both onshore and offshore cases, there is little dependence of these errors on the incidence angle.

The errors $\bar{r}_i^B$ at the seismograms (Fig. 4 and 5) have higher complexity, showing great dependence on the incidence angle and seems to be quite different for the several possible situations. To a better understanding of these errors, it is convenient to separate the trajectory of the wave into two parts and evaluate the errors apart, as done below.

1) Downward + upward refraction: This source of error is due to combination of transmission errors in the downward ray ($\bar{r}_i^A$) with the upward ray. For the onshore models, such errors are very small (assuming that are crossed the

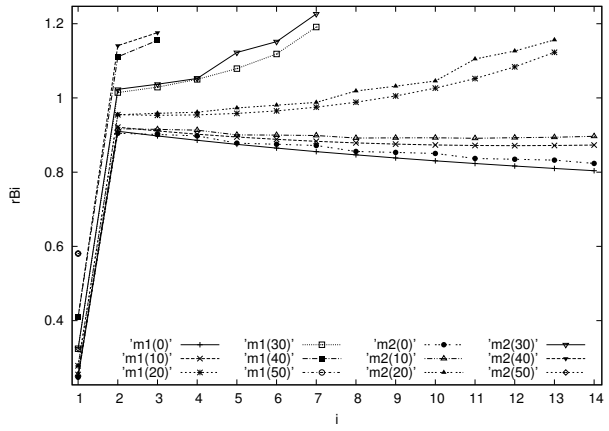

Figure 4: Coefficients $\bar{r}_i^B$ of models 1 e 2 (m1 and m2) per interface, following the Fig. 2.

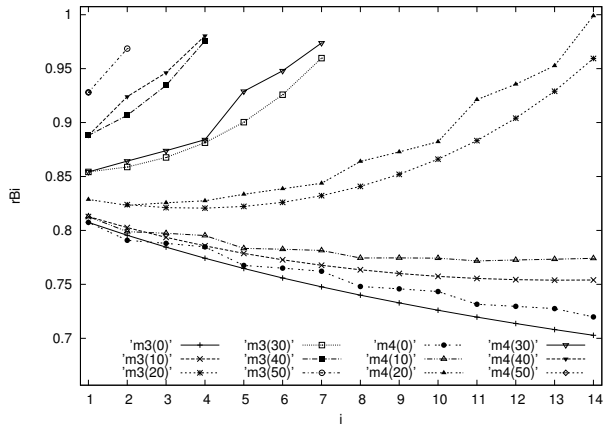

Figure 5: Coefficients $\bar{r}_i^B$ of models 3 e 4 (m3 and m4) per interface, following the Fig. 2.

same layers, with symmetrical angles, in the downward and upward wave, as occurs in plane-parallel layers). This happens because of a compensation of errors $\bar{r}_i^A$ discussed above with corresponding errors of the upward wave. For offshore media, where the wave travel through a large density contrast (water-sediment), such errors are significantly great, substantially contributing to total error. It is important to mention that, just like the error $\bar{r}_i^A$ (downward), this error poorly depends on angle of incidence.

2) Reflection on interface i: The second source of errors if only due to the reflection layer i, and this relative error strongly dependents on the angle (as shown in Fig. 6). Such error make the amplitude of the wave, with regarding of the density contrast increases in relation to wave propagated without regarding this contrast (the coefficient $\bar{r}_i^R$ is less than one). As the angle of incidence (at the first interface) grows, approaching the critical angle at a given layer i, the error tends to decrease, becoming null for angles with values greater than or equal to the critical angle ($\bar{r}_i^R$ becomes one). Logically, in model 2, where inversion layer exists, there is no total reflection on corresponding interfaces, so that the error decreases more

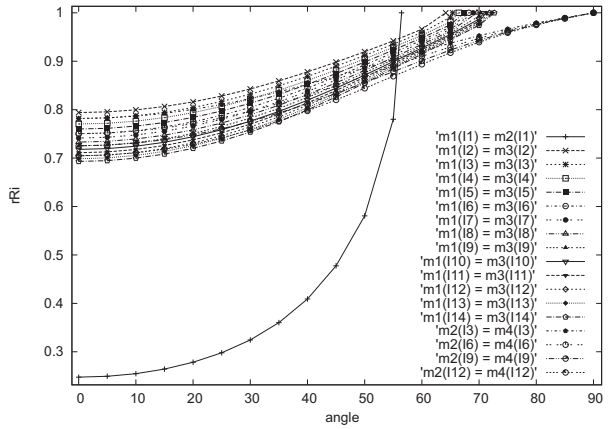

Figure 6: Coefficients $\bar{r}_i^R$ for each model j (mj at labels), shown for some i (Ii) interface, depending on the angle of incidence. The coefficient is defined as $\bar{r}_i^R = R_i^{\rho\ cte}/R_i^{\rho\ var}$.

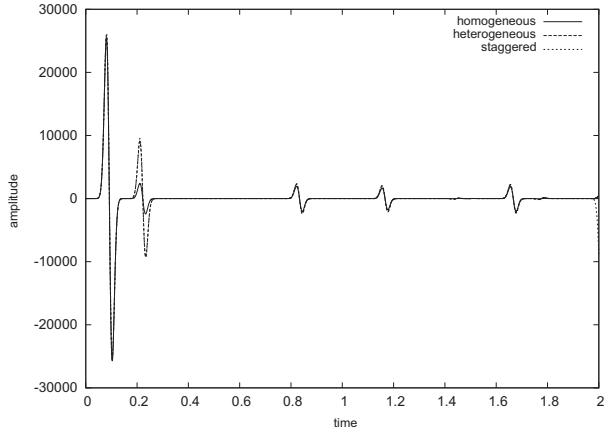

Figure 7: Synthetic seismograms at $z = 380$.

slowly.

Bearing in mind these two sources of error, consider now the total error $\bar{r}_i^B$ on the seismograms. In offshore models, first considering small angles of incidence in the first interface, the error tends to be smaller than the error before reflection ($\bar{r}_i^A$ correspondent), since the two sources of error work in opposite directions. As the angle increases and the error due to reflection decreases, the two sources of error do not tend to be compensated anymore ($\bar{r}_i^B > 1$). In the onshore case, as the angle angle approaches the critical value in a given layer, the second source of error tends to decrease, making the total error decrease, reaching a minimum value for the maximum angle.

NUMERICAL MODELLING

Now, the numerical modelling are presented. At first, plane waves in layered models are modelled, being compared with the analytical results and, in the sequence, the Marmousi offshore model is considered.

Models of Layers

The first model used is formed by five horizontal layers, being the properties of the layers given by $v_1 = 1550$, $\rho_1 = 1000$, $v_2 = 1800$, $\rho_2 = 1800$, $v_3 = 2100$, $\rho_3 = 1900$, $v_4 = 2400$, $\rho_4 = 2000$, $v_5 = 2800$, $\rho_5 = 2100$ (SI units), with the layers interfaces at depths $z_1 = 400$, $z_2 = 510$, $z_3 = 580$, $z_4 = 700$ (in grid points). The numerical parameters used for modelling were: grid interval of $h = 5$m, time interval $\Delta t = 2.5 \times 10^{-4}$ s. The plane wave was generated using the pulse given by the second derivative of Gaussian, characterized by cutoff frequency $f_c = 60$ Hz, applied in the depth $z_i = 370$.

The pressure field was measured along the time in each layer. From the modelled amplitudes, were calculated coefficients of reflection and transmission for each interface. In Figure 7, the seismogram generated (recorded at surface) is shown. The first event of this seismogram corresponds to the direct wave and the others records come from the reflections at the four interfaces. The amplitude of the direct wave is the same for different schemes, since the wave travels only in a homogeneous medium until be registered. The amplitude of the first wave reflected is significantly larger for the modelling with the dynamical schemes, since the density contrast in the first interface is the largest of all. In the other reflections, the difference decreases considerably.

The Table 2 presents the reflection and transmission coefficients obtained directly from the modelled amplitudes above and below of each interface, for the different numerical formulations, together with corresponding theoretical parameters calculated considering or not the density. The results show an excellent agreement between the theoretical and numerical coefficients obtained with the FDM numerical modelling, showing that the implemented schemes are suitable to represent amplitudes consistently.

Table 3: Coefficients B_i and errors. In columns 2-4, this coefficients for the different numerical modelling are shown. The two columns following show the theoretical coefficients with and without consideration of density and in the last three columns, the relative percentual errors in this coefficients with respect to their theoretical coefficients can be seen.

i	B_i numerical			B_i theoretical		relative % error		
	hom	het	stg	hom	het	hom	het	stg
1	0.093	0.356	0.364	0.091	0.367	-1.8	3.1	0.8
2	0.076	0.089	0.089	0.077	0.090	1.9	1.1	0.6
3	0.065	0.078	0.078	0.066	0.079	1.2	1.6	1.2
4	0.074	0.084	0.085	0.075	0.086	1.8	1.8	1.5

In Table 3, the coefficients B_i are presented, calculated from the modelled amplitudes. These coefficients are compared with theoretical coefficients B_i calculated. The results show good agreement with the theoretical values, although, due to the fact that they are accumulated coefficients, they have larger numerical errors than that obtained in a single layer. Logically, decreasing the grid space and the time step, these errors tend to minimize. In addition, the staggered grid has the smallest numerical error and the other two schemes have equivalent error.

Marmousi 2 Model

In this example, it's used a sampled model of the offshore Marmousi model, being the grid sizes given by $Nx \times Nz = 634 \times 334$, with $h = 5$ m. (Fig. 8). Therefore, the model

Table 2: Coefficients of reflection and transmission by layer. The second and third columns shows the reflection coefficient R_i^{hom} and transmission coefficient T_i^{hom} for modelling with the homogeneous formulation. In the following columns are presented, respectively, the coefficients for heterogeneous schemes, staggered, and finally, theoretical.

i	R_i^{hom}	T_i^{hom}	R_i^{het}	T_i^{het}	R_i^{stag}	T_i^{stag}	$R_{i(theo)}^{hom}$	$T_{i(theo)}^{hom}$	$R_{i(theo)}^{het}$	$T_{i(theo)}^{het}$
1	0.093	1.082	0.356	1.361	0.364	1.359	0.091	1.091	0.367	1.367
2	0.078	1.072	0.103	1.099	0.104	1.099	0.077	1.077	0.104	1.104
3	0.067	1.065	0.092	1.090	0.093	1.091	0.067	1.067	0.092	1.092
4	0.077	1.076	0.101	1.100	0.102	1.101	0.077	1.077	0.101	1.101

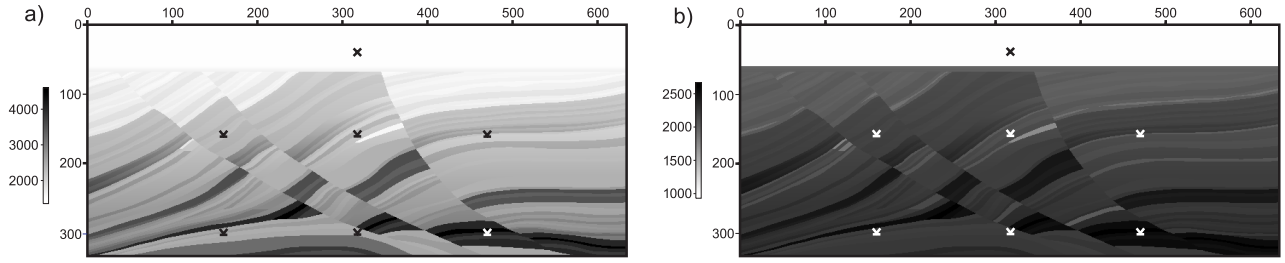

Figure 8: Marmousi 2 model. (a) Velocity v_p and (b) density (SI units). The source and hydrophones positions are showed.

has the total size of $3165\ \mathrm{m} \times 1665\ \mathrm{m}$. The cutoff frequency of the seismic source used was $f_c = 60\ \mathrm{Hz}$ and the time step $\Delta t = 2.5 \times 10^{-4}\ \mathrm{s}$. The source was located at position $x_i = 317$ e $z_i = 40$ of the grid and wave fields were evaluated at points $P_{ij} = (x_i, z_j)$ of the depth $z_1 = 160$ and $z_2 = 300$ for the offset given by $x_1 = 160$, $x_2 = 317$ and $x_3 = 470$.

In Fig. 9, it is shown the variation of the wave field

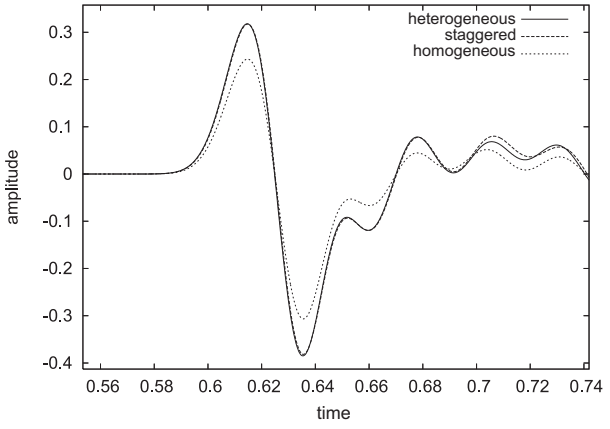

Figure 9: Amplitude of the wave at the point P_{31}.

along the time at the point P_{31} for different operators.In Table 4, the numerical coefficients $\bar{r}A_i$ between the homogeneous scheme and each one of the others two heterogeneous schemes as well as the ratio between them (note that this latter expresses only the errors between the heterogeneous formulations). It is observed that, despite having a complex behavior (as expected), the errors vary between 20 % and 30 %.

CONCLUSIONS

Although simplified, the analytical study of the layers models allowed a better understanding of how the density gradient influences the wave amplitudes, for both onshore and offshore models. The numerical examples presented

Table 4: The r^A coefficients at each P_{ij} point (see text).

coeff	P_{11}	P_{21}	P_{31}	P_{12}	P_{22}	P_{32}
r^A(het)	0.711	0.690	0.731	0.744	0.797	0.721
r^A(stg)	0.714	0.694	0.731	0.747	0.803	0.725
r^A (het/stg)	0.996	0.995	1.000	0.996	0.992	0.994

shown that the FDM schemes implement have provided a reliable amplitude representation for the three approaches.

For the case of complex models, such as Marmousi model, the path of the downward wavefront can be very different from the path of the upward wavefront, so that the transmission errors (downward + upward) have a complex behavior that can vary over the model. Finally, even with all the complexity of real models, we can safely say that the errors in seismic records show significant values, which may exceed 30% in amplitude in depth.

Acknowledgements

L. Di Bartolo wish to thank Faperj and CNPq for the Ph.D. fellowship, and CAPES for the postdoctoral fellowship.

References

Baysal, E., Kosloff, D. D., & Sherwood, J. W. C., 1983. Reverse time migration. *Geophysics*, vol. 48, pp. 1514.

Cohen, G. & Joly, P., 1996. Construction and analysis of fourth-order finite difference schemes for the acoustic wave equation in nonhomogeneous media. *SIAM J. Numer. Anal.*, vol. 33, n. 4, pp. 1266–1302.

Virieux, J., 1986. P-sv wave propagation in heterogeneous media: Velocity-stress finite-difference method. *Geophysics*, vol. 51, pp. 889.